Anomalous spin Josephson effect

Mei-Juan Wang, Jun Wang,* Lei Hao, and Jun-Feng Liu†
Department of Physics, Southeast University, Nanjing 210096, China
and Department of Physics, South University of Science and Technology of China, Shenzhen 518055, China
(Received 1 August 2016; published 28 October 2016)

We report a theoretical study on the spin Josephson effect arising from the exchange coupling of the two ferromagnets (Fs), which are deposited on a two-dimensional (2D) time-reversal-invariant topological insulator. An anomalous spin supercurrent $J_{sz} \sim \sin(\alpha + \alpha_0)$ is found to flow in between the two Fs and the ground state of the system is not limited to the magnetically collinear configuration ($\alpha = n\pi$,n is an integer) but determined by a controllable angle α_0, where α is the crossed angle between the two F magnetizations. The angle α_0 is the dynamic phase of the electrons traveling in between the two Fs and can be controlled electrically by a gate voltage. This anomalous spin Josephson effect, similar to the conventional φ_0 superconductor junction, originates from the definite electron chirality of the helical edge states in the 2D topological insulator. These results indicate that the magnetic coupling in a topological system is different from the usual one in conventional materials.

DOI: 10.1103/PhysRevB.94.155443

I. INTRODUCTION

Spintronics is dedicated to studying spin transports and fabricating spin-based devices, while the first step in this field is to produce spin currents [1] efficiently. Usually, the ferromagnetic metals are utilized to generate spin polarized currents in biased electric circuits, and the ferromagnetic pumping effect [2] is a conventional means of production of pure spin currents. However, these methods of generating spin currents regularly involve high-energy dissipation, which is unfavorable for exploration and application of spin currents in fabricating spin microdevices. Recently, much attention has been paid to the generation of spin currents via spin waves excited in magnetic insulator systems [3–7], where spin transport is believed to be nondissipative.

Besides spin currents of the spin-wave type, the spin Josephson effect was also studied extensively to bring about a dissipationless spin current [7–20] flowing between the two noncollinear magnetizations, which could be a ferromagnetic (F) metal, a ferromagnetic insulator, or even an antiferromagnetic insulator. In some semiconductor systems [19,21,22], different types of spin-orbital interactions were demonstrated to sustain equilibrium spin currents, too. In the magnetic F/F junction, the system has a coupling energy $H_s \sim J_s \mathbf{M}_L \cdot \mathbf{M}_R$, with J_s being the coupling strength and $\mathbf{M}_{L(R)}$ being the left (right) homogeneous magnetization, and thus, the ground state of the junction is the parallel or antiparallel configuration of $\mathbf{M}_L$ and $\mathbf{M}_R$. When the magnetizations are not collinear, a spontaneous spin supercurrent $\mathbf{J}$ flows between them, $\mathbf{J} \sim \mathbf{M}_L \times \mathbf{M}_R$, and the crossed angle α of the two magnetizations is decisive, $J \sim \sin\alpha$. This is also referred to as the spin Josephson effect in the literature [7–12]. Certainly, the spin supercurrent will also precess $\mathbf{M}_L$ and $\mathbf{M}_R$ (Josephson precession), $\partial \mathbf{M}_{L(R)}/\partial t \sim \mathbf{M}_L \times \mathbf{M}_R$; as a result, the F/F junction will ultimately evolve into a collinear structure of $\mathbf{M}_L$ and $\mathbf{M}_R$. However, the spin supercurrent is generally too small to rotate $\mathbf{M}_L$ or $\mathbf{M}_R$ due to the large magnetic stiffness of materials [7].

From the viewpoint of the angular momentum condensation, the antiferromagnetic (AF) insulator [8,9] is much more like a superconductor (S) that is an insulator of the superconducting quasiparticles. Therefore, the exchange coupling of the two insulating AFs can also lead to an equilibrium spin Josephson current [7–9]. Moor *et al.* [8] compared the AF/F/AF junction with the conventional S/F/S junction and showed a great resemblance between these two different junctions; for example, the AF order parameter was also found to oscillate in the middle F layer of the AF/F/AF junction with two different oscillating periodicities, and a *π-state* AF/AF junction was demonstrated to appear within appropriate parameters.

In the superconductor junction, the anomalous Josephson effect [23–29] is a well-known peculiar phenomenon: the supercurrent is given by $J_c \sim \sin(\varphi + \varphi_0)$, with φ being the superconducting phase difference, and the ground state of the junction is not $\varphi = n\pi$ (n, integer) but instead $\varphi = -\varphi_0$. Naturally, the question of whether there is a similar phenomenon in the F/F magnetic junction in which the spin supercurrent has a similar formation $\mathbf{J} \sim \sin(\alpha + \alpha_0)$ arises. This motivates us to study a possible F/F junction producing the anomalous spin Josephson effect.

Given that the conventional φ_0 Josephson junction is often related to the quasiparticles possessing a definite chirality [27,28], we consider here the two F insulators deposited on a two-dimensional topological insulator (2DTI) [29] and utilize the chirality of helical edge states to affect the spin supercurrent. Based on both a lattice model and a low-energy continuum model, we will show that an anomalous spin supercurrent can appear in the F/2DTI/F junction, $J_{sz} \sim \sin(\alpha + \alpha_0)$. The ground state of the junction could be in an arbitrary magnetic configuration determined by the phase α_0, which is affected by the global chemical potential or the local potential in the 2DTI through the gate voltage. The physics is attributed to electrons in the helical edge states possessing a definite chirality and accumulating an uncanceled dynamic phase that modifies the effective crossed angle α of the two F magnetizations.

This work is organized as follows. In Sec. II, the two lattice models of the F/2DTI/F junctions are outlined, and the numerical method for the spin supercurrent is presented. The numerical results of the anomalous spin supercurrent are

*Corresponding author: jwang@seu.edu.cn
†Corresponding author: liujf@sustc.edu.cn

given in Sec. III. A continuum model to interpret the numerical results is addressed in Sec. IV. A brief conclusion is drawn in the last section.

II. MODEL

We take the Kane-Mele graphene model [29] as the prototype of a 2DTI, in which the two opposite spins counterpropagate at the sample boundary, so a pure spin current circulates around the 2DTI system but without a net spin current flowing through the whole sample. Here, we consider two models schematically shown in Fig. 1 by putting the F insulators onto the graphene and study the exchange coupling between them: one is the single-boundary F/2DTI/F junction in which the two Fs are only contacting one boundary of the sample [say, the lower boundary in Fig. 1(a)], and the second is the two-boundary F/2DTI/F junction, where the Fs cover the whole 2DTI system [Fig. 1(b)], so the upper and lower spin helical edge states are supposed to sustain the possible spin supercurrent together.

Since we focus on the equilibrium spin current flowing between the two Fs, the left and right F magnetizations $\mathbf{M}_{L(R)}$ are assumed to be fixed, and the possible rotation of magnetization due to the spin supercurrent is neglected here. The graphene-lattice model of the 2DTI is given by

$$\mathcal{H} = -t\sum_{\langle ij\rangle\sigma} C^{\dagger}_{i\sigma}C_{j\sigma} + \sum_{i\sigma}(V_g(i)-\mu)C^{\dagger}_{i\sigma}C_{i\sigma} + \sum_{i\beta\gamma} C^{+}_{i\beta}(\boldsymbol{\sigma}\cdot\mathbf{M}_i)C_{i\gamma} + i\sum_{\langle\langle lm\sigma\rangle\rangle}\frac{\lambda\nu_{lm}}{3\sqrt{3}}C^{\dagger}_{l\sigma}C_{m\sigma}. \quad (1)$$

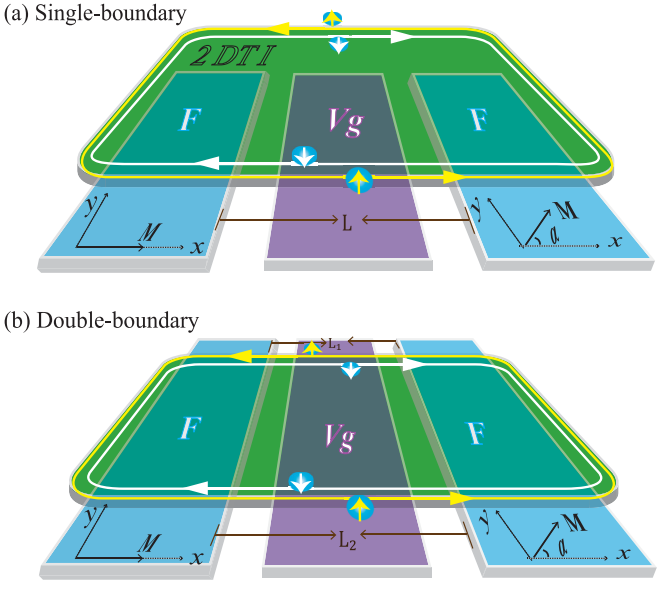

FIG. 1. Schematic of the (a) single-boundary and (b) double-boundary F/2DTI/F junctions. The two uniform F insulators are deposited on the 2DTI with the fixed magnetizations $\mathbf{M}_L$ and $\mathbf{M}_R$, while α denotes the crossed angle between them. A voltage gate V_g is applied to the 2DTI and controls the local potential. The junction length between the two Fs is L in the single-boundary junction, while in the double-boundary case, L_1 and L_2 denote the upper and lower junction lengths.

Here, the first term describes pristine graphene, and only the p_z orbit of the carbon atom is taken into account; $\langle ij\rangle$ stands for the nearest-neighboring sites. $C_{i\sigma(\beta,\gamma)}$ ($C^{\dagger}_{i\sigma(\beta,\gamma)}$) is the creation (annihilation) operator at site i with spin $\sigma(\beta,\gamma)$; μ is the universal chemical potential, and $V_g(i)$ is the local potential that can be modulated by the gate voltage. The third term denotes the spin exchange energy, with $\mathbf{M}_i$ being the magnetization on each site i; the last term is the spin-orbit interaction accounting for the topological phase in graphene with strength λ. $\langle\langle lm\rangle\rangle$ denotes the next-nearest-neighboring sites, and $\nu_{lm}=1$ if the next-nearest-neighboring hopping is counterclockwise, while $\nu_{lm}=-1$ if it is clockwise with respect to the normal of the 2D sheet.

It is assumed that a homogeneous magnetization $\mathbf{M}_{L(R)}$ is induced in the left (right) F region through the magnetic proximity effect in the model of Fig. 1. The spin quantum axis is taken along the z direction, and s_z is a good quantum number in the original Kane-Mele model without any magnetization. The magnetization $\mathbf{M}_{L(R)}$ is assumed to be in the xy plane with a crossed angle α. First, the spin supercurrent from the exchange coupling between the two Fs, $\mathbf{M}_L\times\mathbf{M}_R$, is polarized along the z direction, and thus, J_{sz} flowing along the sample boundary is conserved. However, the $s_{x(y)}$ spin supercurrent $J_{sx(sy)}$ with polarization perpendicular to the z axis is not a conserved quantity and instead varies in space due to the spin-orbital interaction. Second, the planar magnetization will open an energy gap of the helical spin states of the 2DTI, so the original spin currents circulating the 2DTI will be interrupted, and the spin current flowing between the two Fs, if present, will come from the magnetization exchange effect.

We consider the spin supercurrent flowing in the F/2DTI/F junction in equilibrium, and no bias is applied to the system. Without loss of generalization, $\mathbf{M}_L$ is set along the x axis $(M_L, 0)$, and $\mathbf{M}_R$ has a planar crossed angle upon the x axis $(M_R\cos\alpha, M_R\sin\alpha)$. Since σ_z spin current is conserved, one is allowed to evaluate it at any interface of the junction [27],

$$J_{sz} = \frac{\hbar}{2}\int\frac{dE}{2\pi}\mathrm{Tr}[\sigma_z G^{<}_{l,l+1}(E)\tilde{t}_{l+1,l} - \mathrm{H.c.}], \quad (2)$$

where $G^{<}(E)$ is the lesser Green's function, the subscript l is the index of the unit slice of the graphene lattice, $\tilde{t}_{l+1,l}$ is the hopping matrix between neighboring slices, and the trace is over the unit slice. At equilibrium, $G^{<}=[G^a-G^r]f(E)$, where $G^{r(a)}$ is the retarded (advanced) Green's function and f is the Fermi-Dirac distribution function. It is emphasized that the thermal equilibrium case is considered here, and only those states below the chemical potential μ contribute to the supercurrent at zero temperature $T=0$ K.

Generally speaking, the static potential landscape in the junction shall not be uniform due to the magnetic proximity effect. Here, this potential can be simulated by the adjustable $V_g(i)$ as well as the universal chemical potential μ, both of which can, in principle, be modulated by gate voltages. For simplicity, a uniform $V_g(i)$ is applied only to the middle nonmagnetic region of the F/2DTI/F junction. In Eq. (2), we count the spin current J_{sz} flowing through the whole sample, where no net s_z spin current is expected when the pure 2DTI is considered without magnetization. Therefore, the nonzero J_{sz} flowing in the junction will come from the exchange coupling between the two Fs.

III. NUMERICAL RESULTS

In this section, we will present the numerical results of the spin supercurrent J_{sz} flowing in the F/2DTI/F junction. In the numerics, the magnitudes of $\mathbf{M}_L$ and $\mathbf{M}_R$ are assumed to be equal in a unit of energy, $M = 5$ Mev; the hopping energy is set as $t = 1$ eV, the spin-orbital interaction is $\lambda = 0.05$ eV, and the temperature is set as $T = 0$ K. Here, $M_{L(R)} \ll \lambda$ is considered because we aim to study only the helical edge electrons with a definite chirality contributing to the spin Josephson effect and neglect the bulk states contributing to the spin supercurrent, which is expected not to bring about any new result.

We first calculate the single-boundary F/2DTI/F junction [Fig. 1(a)] and present the current-phase relationship $J_{sz}(\alpha)$ in Fig. 2(a) with different local potentials V_g, which is assumed to be homogeneous in the middle 2DTI region. In calculations, the chemical potential is set as $\mu = 0$, so that the left and right F regions have a particle-hole symmetry similar to that of a superconductor system. It is shown in Fig. 2(a) that a nonzero spin supercurrent J_{sz} arises to flow between the two Fs. The whole profile of curves deviates from a perfect sine function, and this is due to the high transparency of the junction [in the one-dimensional (1D) transport of the helical edge state, the transmission of electrons approaches the unit 1 due to the Klein-Gordon paradox]. When $V_g = 0$, the spin supercurrent fulfills $J_{sz}(\alpha = n\pi) = 0$ (n is an integer). When $V_g \neq 0$, the J_{sz} curve seems to shift to a nonzero angle α_0, so it can be expressed as $J_{sz} \sim \sin(\alpha + \alpha_0)$.

The peculiar phenomenon of the spin supercurrent J_{sz}, a nonzero spin supercurrent flowing between the two collinear magnetizations, can be referred to as the anomalous spin Josephson effect, like the conventional φ_0 Josephson junction [23]. Here, α_0 shall also depend on the junction length L in addition to the local potential V_g since it is expected that both of them (V_g, L) are significant to this phase α_0. In Figs. 2(b) and 2(c), we depict $J_{sz}(\alpha = 0)$ as a function of L and V_g, respectively. It is seen that the anomalous spin supercurrent $J_{sz}(\alpha = 0)$ displays clear periodic oscillations with either L or V_g but dampens with the junction length L. This is related to the $\mu = 0$ used in our calculations, under which the left and right Fs are insulating for the electrons of the helical edge state. Here, $\xi_m = \hbar v_F / M$ is the magnetic coherence length of the quasiparticle (excitation of the magnetized helical edge state of the 2DTI), with v_F being the electron velocity of the helical states, which is estimated to be $\hbar v_F = 3\lambda/2a\pi$, with a being the lattice constant.

We continue to study the two-boundary model in Fig. 1(b) in which the two Fs cover the whole 2DTI sample, and both the upper and lower helical spin states are involved in the spin transport. Simply, electrons in the middle 2DTI layer of the F/2DTI/F junction will have no chirality due to the two offset edge states involved. In Fig. 3(a), the spin current-phase relationship is plotted with different local potentials V_g, where V_g is applied to both boundaries and the upper and lower boundaries have the same length $L_1 = L_2 = L$. One can see that there is no anomalous spin supercurrent and the spin supercurrent fulfills $J_{sz}(\alpha = n\pi) = 0$. Although the variation of V_g or L may lead to the spin supercurrent reversing and, in fact, the curves within $V_g = \pm M$ exhibit a typical current-phase relation profile of the π-state Josephson junction, the nonzero voltage (V_g) does not trigger any nonzero spin supercurrent $J_{sz}(\alpha = 0) \neq 0$ in the collinear configuration

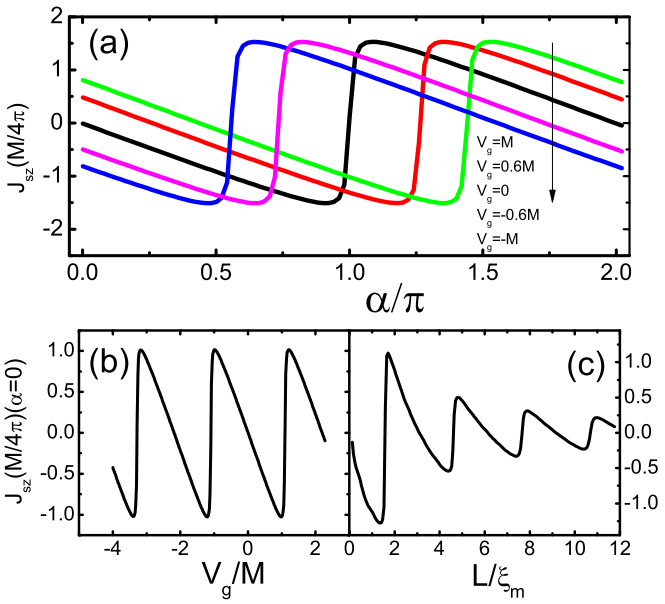

FIG. 2. (a) Spin supercurrent J_{sz} versus the crossed angle α in the single-boundary F/2DTI/F junction with different voltages. Anomalous spin current $J_{sz}(\alpha = 0)$ as a function of (b) the voltage V_g and (c) the junction length L. Parameters are $L = \xi_m$ in (a), $L = 3\xi_m$ and $\alpha = 0$ in (b), and $V_g = 1.4M$ and $\alpha = 0$ in (c), and others are described in text.

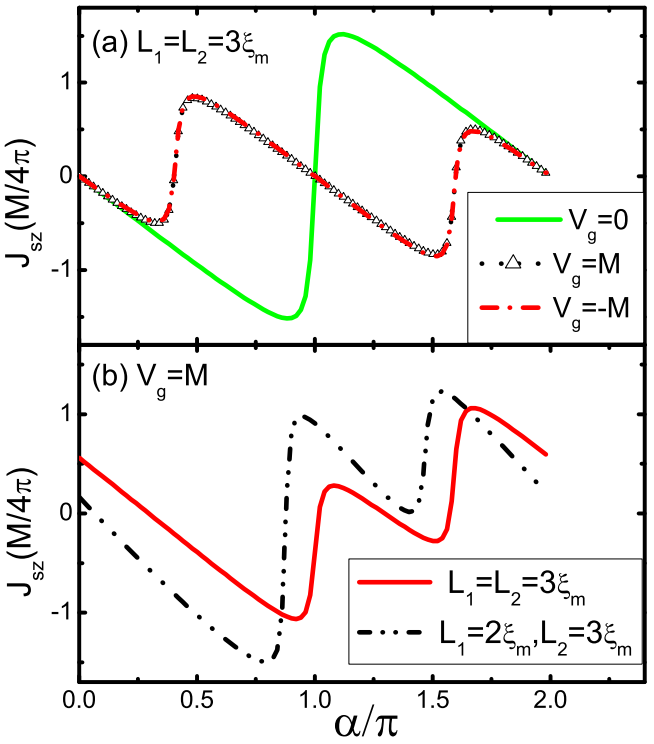

FIG. 3. Spin supercurrents J_{sz} versus the crossed angle α in the double-boundary F/2DTI/F junction with the different (a) voltages and (b) junction lengths L. In (b), the voltage is applied only to a single edge of the 2DTI for the solid curve and to both edges for the dash-dotted line.

of the two Fs. The current reversal can also be regarded as a π state of the F/F junction [8], similar to the usual π-state Josephson junction [30]. Obviously, only the electron chirality can account for the difference in Figs. 2(a) and 3(a).

The anomalous spin supercurrent in this double-boundary junction can be recovered when the symmetry between the upper and lower boundaries of the junction is broken. Figure 3(b) confirms that a nonzero spin supercurrent appears at the zero crossed angle ($\alpha = 0$). Here, two different cases are considered: one case (the solid curve) is that the gate voltage V_g is applied to only one boundary (but not the both), while the other one (dash-dotted curve) is that different boundary lengths $L_1 \neq L_2$ are taken in the calculations. So the anomalous spin Josephson effect occurs again, but the symmetry of $J_{sz}(\alpha) = -J_s z(-\alpha + n\pi)$ is broken. As a matter of fact, the current-phase relationship in Fig. 3(b) can be regarded as the summation of the two different α_0-state F/2DTI/F junctions. This will be interpreted in the following section.

IV. CONTINUUM MODEL

The above results show that the exchange coupling between two Fs via the 2DTI is sufficiently different from that in the usual F/F case, and it may even take its maximum in the parallel F structure. To account for these numerical results, we consider the following 1D low-energy continuum model, which is based on the magnetized helical edge state of the 2DTI [31]:

$$H_s = [-i\hbar v_F \partial/\partial_x + V_g(x) - \mu]\sigma_z\tau_z + M(\sigma_x \cos\alpha + \sigma_y \sin\alpha). \quad (3)$$

Here, the first term is the massless Dirac equation describing the 1D helical edge state, and the second term denotes the planar magnetization $(M\cos\alpha, M\sin\alpha)$ in the unit of energy, which is assumed from the magnetic proximity effect by depositing the F insulator on the 2DTI. $\sigma_{x,y,z}$ is the spin operator, $\tau_z = \pm 1$ denotes the opposite chiralities of electrons, μ is the global chemical potential in the whole junction system, and $V_g(x)$ stands for the potential landscape. One can see that there is not much difference between V_g and μ in controlling the electron momentum.

The eigenvalue and eigenfunction of the above Hamiltonian with a constant V_g are given by

$$E = \mu - V_g \pm \sqrt{M^2 + \hbar^2 v_F^2 k_x^2} \quad (4)$$

and

$$\psi_\pm(\tau_z) = \frac{1}{\sqrt{V}} \begin{pmatrix} \sqrt{\frac{E' \pm \tau_z \Omega}{2E'}} e^{i\alpha/2} \\ \sqrt{\frac{E' \mp \tau_z \Omega}{2E'}} e^{-i\alpha/2} \end{pmatrix} e^{ik_x x}, \quad (5)$$

respectively, where $\Omega = \sqrt{(E')^2 - M^2}$, with $E' = E - \mu + V_g$, and V is volume. It is seen that when $\mu = V_g = 0$, the system has particle-hole symmetry, and Eq. (3) is the same as a mean-field superconductor Hamiltonian describing a superconducting state sustained by the helical edge state [31]. From Eq. (4), there is an energy gap opened by the planar magnetization M that couples the up and down spins, so the magnetization M plays a role similar to that of the superconducting pair potential coupling the electron and hole. However, the distinction of Eq. (4) from the energy spectrum of superconducting quasiparticles is that the energy gap of the magnetized 2DTI system is not fixed around μ.

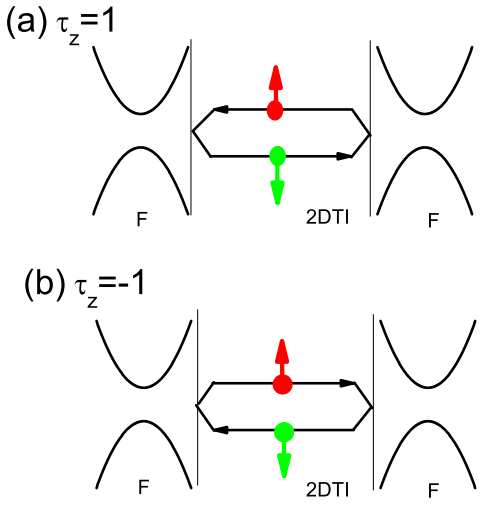

FIG. 4. Schematic of a self-closed path of quasiparticles reflected on the left and right interfaces of the F/2DTI/F junction. Two opposite chiralities are plotted in (a) and (b).

We now calculate the bound-state energy in the single-boundary F/2DTI/F junction and consider the chemical potential residing in the energy gap $|\mu| < M$ and constant V_g applied merely to the middle nonmagnetic 2DTI region. Since only evanescent waves are possible in the left and right F regions, the quasiparticle scattering at the left interface F/2DTI ($x = 0$) and the right interface 2DTI/F ($x = L$) will constitute a self-closed path, as schematically illustrated in Fig. 4. There are two possible closed paths, $\tau_z = 1$ and $\tau_z = -1$, representing the clockwise and counterclockwise traveling of electrons in the 2DTI. In other words, the model in Fig. 4(b) represents the case of the lower helical edge state sustaining the 1D F/2DTI/F junction if Fig. 4(a) is based on the upper helical edge state of a 2DTI. We use the secular equation [32]

$$\mathrm{Det}|1 - r(L)r'(0)| = 0, \quad (6)$$

where $r(L)$ and $r'(0)$ are Andreev-like reflection coefficients of spins at the interface ($x = L$) of F/2DTI and the $x = 0$ interface of 2DTI/F, respectively. $r(L) = \sqrt{\frac{E'-\Omega}{E'+\Omega}} e^{-i\alpha} p, r'(0) = \sqrt{\frac{E'-\Omega}{E'+\Omega}}$, where $p = e^{2i\tau_z E' L/\hbar v_F}$ denotes an accumulated dynamic phase when electrons propagate in the middle nonmagnetic 2DTI region. Within direct algebra, we obtain the transcendental equation of the possible bound state in the energy gap $|E| < M$,

$$E - \mu = \pm M \cos[\alpha/2 + \tau_z(E - \mu + V_g)L/\hbar v_F]. \quad (7)$$

This represents the ground-state energy of the single-boundary F/2DTI/F junction and is similar to the Andreev bound state of a superconductor junction. But the difference is clear: the chemical μ in a superconductor junction will not enter this $E(\alpha)$ relationship directly because the energy spectrum of a superconductor always fulfills the particle-hole symmetry. However, the bound state energy of the above equation is

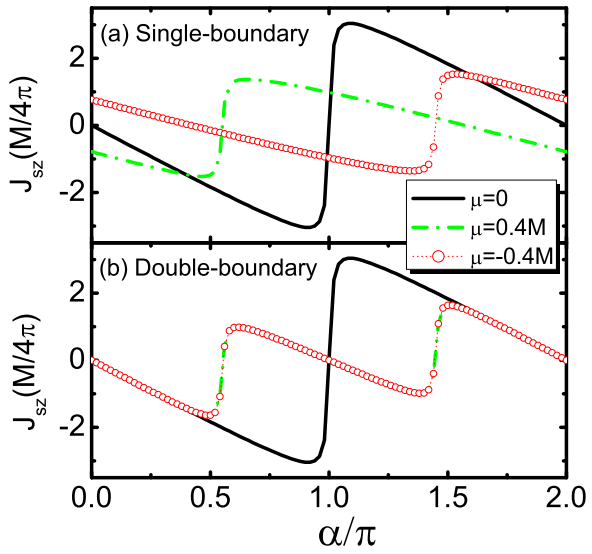

FIG. 5. Spin supercurrent in the (a) single-boundary and (b) double-boundary F/2DTI/F junction as a function of the crossed angle α with different chemical potentials. Parameters are $V_g = 0$ and $L_1 = L_2 = L = \xi_m$.

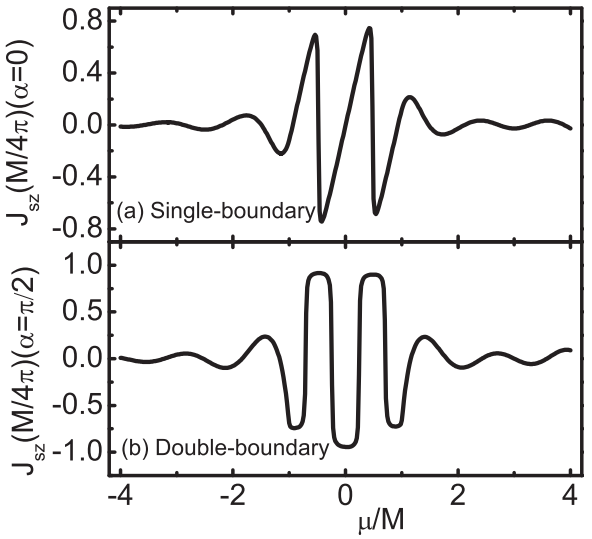

FIG. 6. (a) Anomalous spin supercurrent $J_{sz}(\alpha = 0)$ in the single-boundary junction versus the chemical potential μ and (b) the spin supercurrent $J_{sz}(\alpha = \pi/2)$ in the double-boundary junction. Parameters are $V_g = 0$ and $L = L_1 = L_2 = 3\xi_m$.

not fixed at the chemical potential. When $\xi_m \ll L$, the bound state is simplified as $E(\tau_z) = \mu \pm M\cos(\alpha/2 + \alpha_0)$, and this allows one to evaluate the spin current, $J_{sz} = \frac{\hbar}{2}(\partial E/\partial\alpha) \sim \sin(\alpha/2 + \alpha_0)$,$\alpha_0 = \tau_z(\mu - V_g)L/\hbar v_F$. Therefore, it is seen that in the single-boundary junction (either $\tau_z = 1$ or $\tau_z = -1$ is taken into account), there will be a nonzero spin supercurrent at a zero crossed angle ($\alpha = 0$) between the left and right Fs, as long as μ or V_g is nonzero. When both $\tau_z = 1$ and $\tau_z = -1$ are taken into account in the double-boundary F/2DTI/F junction, the anomalous spin supercurrent will vanish, $J_{sz} \sim \sum_{\tau_z} \sin(\alpha/2 + \tau_z\alpha_0)$ and $J_{sz}(\alpha = n\pi) = 0$. This can entirely account for the difference between the current-phase relationships of the one-boundary and double-boundary junctions, as shown in Figs. 2 and 3.

From the above bound state $E(\alpha)$, one can see that the chemical potential μ plays role nearly similar to that of the voltage V_g in modulating the spin supercurrent J_{sz}. To confirm this, we proceed to compute J_{sz} with the variation of μ by using the same lattice model in Eq. (1). Both the single- and double-boundary F/2DTI/F junctions are calculated, and results are presented in Fig. 5, where the voltage is set to vanish ($V_g = 0$). In Fig. 5(a), where the single-boundary case is studied, the anomalous spin supercurrent is shown to appear at $\alpha = 0$. Opposite $+\mu$ and $-\mu$ will lead to opposite phase shifts of $J_{sz}(\alpha)$, as indicated by the dot-dashed line and circles. However, there is no such anomalous spin Josephson effect [$J_z(\alpha = 0) = 0$] in the double-boundary case, as shown Fig. 5(b). Certainly, the system is assumed to have mirror symmetry, i.e., $V_g = 0$ and $L_1 = L_2$. The reason is that in the double-boundary case, both $\tau_z = \pm 1$ electrons contribute to the spin supercurrent. So it is not strange that the two curves $\mu = -0.4M$ and $\mu = 0.4M$ overlap with each other exactly as shown in Fig. 5(b). Actually, the same phenomenon appears in the solid and dotted lines in Fig. 3(a), where opposite $V_g = \pm M$ are computed in the double-boundary F/2DTI/F junction.

In Fig. 6(a), we plot the anomalous current $J_{sz}(\alpha = 0)$ as a function of μ, and a clear oscillation is seen. This is similar to the result of $J_{sz}(\alpha = 0)$ versus V_g in Fig. 2(b), However, the difference between V_g and μ in modulating $J_{sz}(\alpha = 0)$ is also clear: the chemical potential μ not only brings about a phase shift α_0 in the current-phase relationship of $J_{sz}(\alpha + \alpha_0)$ but also significantly affects the magnitude of J_{sz}. At zero temperature, the variation of μ will change the states below it, contributing to the current integral of Eq. (2); for example, when $|\mu| > M$, no bound state in the energy gap contributes to J_{sz}, and only the continuum spectrum does, so the magnitude of J_{sz} will decrease rapidly. This is clearly seen by comparing Fig. 6(a) with Fig. 2(b). In fact, the continuum spectrum can only lead to a negligible size of the equilibrium spin supercurrent because the phases of the scattering coefficients r and r' change rapidly with the energy E. It is also for this reason that not only do the $J_{sz}(\alpha)$ curves in Fig. 5(a) exhibit a phase shift [like the case of V_g variation in Fig. 2(a)] when μ is changed, but the curve profiles have changed a little in comparison to the $\mu = 0$ curve. At $\mu = \pm 0.4M$, only part of the bound states $E(\alpha)$ of Eq. (7) contributes to J_{sz}, and the continuum spectrum's contribution will increase gradually; as a result, J_{sz} varies very slowly within some interval of the crossed angle α.

In Fig. 6(b), the magnitude of J_{sz} in the double-boundary F/2DTI/F junction is plotted as a function of μ, and similarly, $J_{sz}(\alpha = \pi/2)$ shows a clear oscillation with μ. One can see that when $|\mu| > M$, the magnitude of J_{sz} exhibits a rapid reduction, too, because the discrete bound states in the energy gap $|\mu| < M$ are gradually precluded when the chemical potential μ is shifted away from the particle-hole symmetry point $\mu = 0$. Figure 6(b) also shows that the spin supercurrent direction can be reversed regularly and $J_{sz}(\mu) = J_{sz}(-\mu)$. The current reversal indicates that the ground state of the F/2DTI/F junction should alternate in the antiparallel ($\alpha = \pi$) and parallel ($\alpha = 0$) configurations of two Fs. which is the same as

the conventional 0-π state transition of a Josephson junction. The antisymmetry relation $J_{sz}(\alpha = 0, \mu) = -J_{sz}(\alpha = 0, -\mu)$ in Fig. 6(a) coincides with the derived result of $\alpha_0 = \mu L/\hbar v_F$.

In Eq. (7), one can see that a zero-energy mode $E - \mu = 0$ always exists in the studied F/2DTI/F junction, which is similar to the Majorana zero-energy mode in a topological superconductor junction [31]. This directly indicates that J_{sz} should display a 4π-periodicity current-phase relationship, $J_z \sim \sin\alpha/2$. However, we failed to recover this phenomenon in our numerical calculations because an equilibrium case is considered here, and moreover, the 4π-periodicity prediction is based on the assumption of metastable states contributing to the current. For example, both bound states, $E \sim \pm M\cos(\alpha/2 + \alpha_0)$, will contribute to J_{sz} together in equilibrium as long as $E - \mu < 0$, so that only 2π periodicity is seen. Actually, the two bound states in Eq. (7) may represent different symmetries of the junction like the Andreev bound states in a topological Josephson junction, which stand for different particle parities; a 4π-periodicity spin supercurrent is possible only if the system is always in a single bound state, $E \sim -\cos(\alpha/2 + \alpha_0)$ or $E \sim +\cos(\alpha/2 + \alpha_0)$. This fractional spin Josephson effect was studied in detail in Ref. [33], in which two Fs were supposed to stand on the edges of two independent TIs.

V. CONCLUSION

We have investigated the spin Josephson effect in the F/2DTI/F junction and focused on the helical edge states of the 2DTI sustaining the spin transport. Based on both a lattice model and a continuum model, we showed that a nonzero spin supercurrent can flow in the parallel magnetic structure of the junction ($\alpha = n\pi$), $J_{sz} \sim \sin(\alpha + \alpha_0)$, which is contrary to the usual spin Josephson effect ($\alpha_0 = 0$). According to the low-energy continuum model, we demonstrated that this anomalous spin Josephson effect is due to the definite chirality of electrons in the 2DTI generating an uncanceled dynamic phase accumulation α_0 when electrons travel between the two Fs. This onset phase α_0 was shown to be modulated by varying either a local static potential or the universal chemical potential via gate voltages. Our findings indicate also that the magnetic coupling in a topological (spin-Chern) system is very different from that through conventional media.

ACKNOWLEDGMENTS

The work described in this paper is supported by the NSFC (Grants No. 11274059, No. 11574045, and No. 11204187) and the NSF of Jiangsu Province (Grant No. BK20131284).

[1] S. Maekawa, H. Adachi, K. Uchida, J. Ieda, and E. Saitoh, J. Phys. Soc. Jpn. **82**, 102002 (2013).
[2] Y. Tserkovnyak, A. Brataas, and G. E. W. Bauer, Phys. Rev. Lett. **88**, 117601 (2002).
[3] H. Wu, C. H. Wan, X. Zhang, Z. H. Yuan, Q. T. Zhang, J. Y. Qin, H. X. Wei, X. F. Han, and S. Zhang, Phys. Rev. B **93**, 060403(R) (2016).
[4] S. M. Rezende, R. L. Rodríguez-Suárez, and A. Azevedo, Phys. Rev. B **93**, 054412 (2016).
[5] L. J. Cornelissen, J. Liu, R. A. Duine, J. Ben Youssef, and B. J. van Wees, Nat. Phys. **11**, 1022 (2015).
[6] Y. Tserkovnyak, Nat. Nanotechnol. **8**, 706 (2013); S. Takei and Y. Tserkovnyak, Phys. Rev. Lett. **112**, 227201 (2014); K. Nakata, K. A. van Hoogdalem, P. Simon, and D. Loss, Phys. Rev. B **90**, 144419 (2014).
[7] W. Chen, P. Horsch, and D. Manske, Phys. Rev. B **89**, 064427 (2014).
[8] A. Moor, A. F. Volkov, and K. B. Efetov, Phys. Rev. B **85**, 014523 (2012).
[9] D. Chassé and A.-M. S. Tremblay, Phys. Rev. B **81**, 115102 (2010).
[10] Y.-L. Lee and Y.-W. Lee, Phys. Rev. B **68**, 184413 (2003).
[11] F. S. Nogueira and K.-H. Bennemann, Europhys. Lett. **67**, 620 (2004).
[12] P. Bruno and V. K. Dugaev, Phys. Rev. B **72**, 241302(R) (2005).
[13] J. König, M. C. Bønsager, and A. H. MacDonald, Phys. Rev. Lett. **87**, 187202 (2001).
[14] H. Katsura, N. Nagaosa, and A. V. Balatsky, Phys. Rev. Lett. **95**, 057205 (2005).
[15] P. Chandr, P. Coleman, and A. I. Larkin, J. Phys. Condens. Matter **2**, 7933 (1990).
[16] M. Braun, J. Konig, and J. Martinek, Superlattices Microstruct. **37**, 333 (2005).
[17] H. Zhang, Z. Ma, and J.-F. Liu, Sci. Rep. **4**, 6464 (2014).
[18] A. Schillinga and H. Grundmann, Ann. Phys. (N.Y.) **327**, 2301 (2012).
[19] J. Wang and K. S. Chan, Phys. Rev. B **74**, 035342 (2006).
[20] B. Wang, J. Peng, D. Y. Xing, and J. Wang, Phys. Rev. Lett. **95**, 086608 (2005).
[21] E. I. Rashba, Phys. Rev. B **68**, 241315(R) (2003).
[22] E. B. Sonin, Adv. Phys. **59**, 181 (2010).
[23] A. Buzdin, Phys. Rev. Lett. **101**, 107005 (2008).
[24] A. Zazunov, R. Egger, T. Jonckheere, and T. Martin, Phys. Rev. Lett. **103**, 147004 (2009).
[25] H. Sickinger, A. Lipman, M. Weides, R. G. Mints, H. Kohlstedt, D. Koelle, R. Kleiner, and E. Goldobin, Phys. Rev. Lett. **109**, 107002 (2012).
[26] J.-F. Liu and K. S. Chan, Phys. Rev. B **82**, 125305 (2010); **82**, 184533 (2010).
[27] J. Wang, L. Hao, and J.-F. Liu, Phys. Rev. B **93**, 155405 (2016).
[28] Y. Tanaka, T. Yokoyama, and N. Nagaosa, Phys. Rev. Lett. **103**, 107002 (2009); A. M. Black-Schaffer and J. Linder, Phys. Rev. B **83**, 220511(R) (2011).
[29] C. L. Kane and E. J. Mele, Phys. Rev. Lett. **95**, 226801 (2005).
[30] A. A. Golubov, M. Y. Kupriyanov, and E. Il'ichev, Rev. Mod. Phys. **76**, 411 (2004).
[31] L. Fu and C. L. Kane, Phys. Rev. B **79**, 161408(R) (2009).
[32] C. W. J. Beenakker, Phys. Rev. Lett. **67**, 3836 (1991).
[33] Q. Meng, V. Shivamoggi, T. L. Hughes, M. J. Gilbert, and S. Vishveshwara, Phys. Rev. B **86**, 165110 (2012).